To be published in Proc. EUSIPCO'96, Trieste, Italy

EQUALIZERS FOR TRANSMULTIPLEXERS IN ORTHOGONAL MULTIPLE CARRIER DATA TRANSMISSION

Thomas Wiegand[1] *and Norbert J. Fliege*[2]

[1]Telecommunications Institute
University of Erlangen-Nuremberg
Cauerstr. 7/NT, 91058 Erlangen, Germany
wiegand@nt.e-technik.uni-erlangen.de

[2]Telecommunications Institute
Hamburg University of Technology
Eissendorfer Str. 40, 21071 Hamburg, Germany
fliege@tu-harburg.d400.de

ABSTRACT

Orthogonal multiple carrier data transmission systems are efficiently realized using modified DFT transmultiplexer filter banks. In data transmission applications, a non-ideal transmission channel causes distortions such as intersymbol interference and crosstalk between the subrate bands of the transmultiplexer. Hence, in order to equalize these distortions, subband equalizers, which affect the intersymbol interference and crosstalk behavior, are considered for implementation. The special structure of modified DFT transmultiplexers requires a discussion concerning the various possibilities of placing the subband equalizers at the receiver. Wiener solutions and LMS adaptive algorithms for various new subband equalizer structures are derived and compared by means of simulation results.

1 INTRODUCTION

In [1] a novel orthogonal multiple carrier (OMC) data transmission system is presented, which is based on a computationally efficient implementation of a modified DFT (MDFT) transmultiplexer filter bank. The MDFT transmultiplexer filter bank provides almost perfect reconstruction, i.e. intersymbol interference within the subbands and crosstalk between the subbands can be kept arbitrarily small [2].

In order to accomplish almost perfect reconstruction, the filters employed in an M-band MDFT filter bank are computed using a linear phase prototype FIR filter $h(n)$, which produces by convolution with itself a linear phase impulse response, that satisfies the Nyquist criterion each $n = mM$ samples. Furthermore, the prototype filter is modulated, resulting in linear phase impulse responses

$$g_\mu(n) = M \cdot h(n) e^{j\Omega_\mu n}, \quad \mu = 0, 1, 2 \ldots M-1 \qquad (1)$$

for the synthesis filters as well as for the analysis filters

$$h_\nu(n) = h(n) e^{j\Omega_\nu n}, \quad \nu = 0, 1, 2 \ldots M-1 \qquad (2)$$

with $\Omega_\mu = \mu 2\pi/M$ and $\Omega_\nu = \nu 2\pi/M$. By restricting the bandwidth of $h(n)$ to the normalized cutoff frequency $2\pi/M$, the subbands are only overlapping with their adjacent subbands and, as assumed in the paper, the crosstalk is restricted to that neighborhood. For detailed information on MDFT filter bank design see [3].

Notations. Vectors are indicated by small, matrices by capital bold faced letters. The superscripts $*, t$ and $\dagger$ denote complex conjugation, transposition and Hermitian transposition, respectively. The separation of a complex signal into its real and imaginary part is denoted by the subscripts r and i, respectively.

2 CONFIGURATION

Basically, an M-band MDFT transmultiplexer consists of an interleaver, an up-sampler by $M/2$, a synthesis filter bank, an analysis filter bank, a down-sampler by $M/2$, and a deinterleaver. In what follows, a system description of the MDFT transmultiplexer, suitable for understanding the various subband equalizer approaches below, is given. For sake of simplicity, we use the direct implementation of the MDFT transmultiplexer as depicted in Fig. 1, since the direct implementation can be modified to the computationally efficient implementation of [1] by simply shifting the system components.

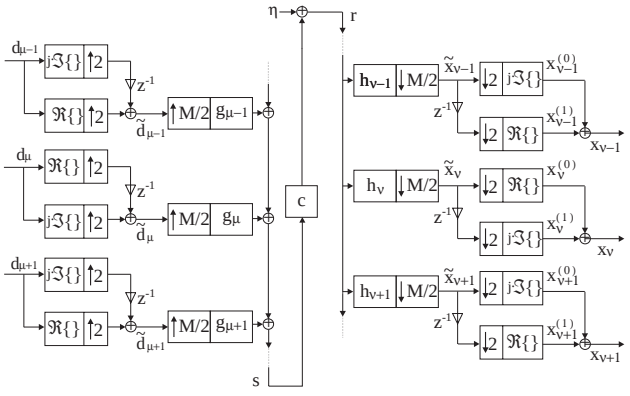

Figure 1: Detail of an M-band MDFT transmultiplexer filter bank in direct implementation realizing an OMC data transmission system.

Given a complex signal $d_\mu(m)$ that is fed at samp-

ling rate m into the μ'th subband of the interleaver, the corresponding output signal can be written as

$$\tilde{d}_\mu(2m+1-\kappa) = \frac{1}{2}\left(d_\mu(m) + (-1)^{\mu+\kappa} d^*_\mu(m)\right), \quad (3)$$

where $\kappa \in \{0,1\}$[1]. By substituting $k = 2m+1-\kappa$, we obtain the output signal of the synthesis filter bank having a sampling rate of $n = kM/2$ as follows

$$s(n) = \sum_{\mu=0}^{M-1} \sum_{k=-\infty}^{\infty} \tilde{d}_\mu(k) g_\mu(n - kM/2). \quad (4)$$

The signal $s(n)$ is fed into the transmission channel that is modeled as a cascade of a linear filter $c(n)$ and a discrete additive noise process $\eta(n)$ producing the signal $r(n) = s(n) * c(n) + \eta(n)$ at the receiver side, where "$*$" denotes convolution. For simplicity reasons, we set $\eta(n) = 0$ for the rest of this chapter.

By defining a subband transfer function

$$f_{\mu,\nu}(n) \stackrel{\triangle}{=} g_\mu(n) * c(n) * h_\nu(n), \quad (5)$$

and taking into account the down-sampling by $M/2$ at the receiver, we obtain

$$\tilde{x}_\nu(k) = \sum_{\mu=0}^{M-1} \sum_{l=-\infty}^{\infty} \tilde{d}_\mu(l) f_{\mu,\nu}((k-l)M/2). \quad (6)$$

Using the deinterleaver we finally get[2]

$$x_\nu(m) = \frac{1}{2}\sum_{\lambda=0}^{1} \tilde{x}_\nu(2m-\lambda) + (-1)^{\nu+\lambda}\tilde{x}^*_\nu(2m-\lambda). \quad (7)$$

The conditions of almost perfect reconstruction for the MDFT transmultiplexer filter bank can be illustrated using the subband transfer function, defined by (5). Interestingly, the signal $\tilde{x}_\mu(k)$ at the receiver and the corresponding signal $\tilde{d}_\mu(k)$ at the transmitter are not equal valued even if the conditions for almost perfect reconstruction are satisfied, i.e. $c(n) = \delta(n)$, $\eta = 0$ and the usage of the filter bank design delineated above. More precisely, assuming these conditions, if $\tilde{d}_\mu(k)$ is for example real valued, the same real value is preserved in $\tilde{x}_\mu(k)$, whereas the imaginary value of $\tilde{x}_\mu(k)$ is modified. This is due to the fact that the subband transfer functions satisfy the generalized Nyquist criterion at sampling positions $n = mM$ and that they are strictly real valued at sampling positions $n = mM + M/2$. The signal $x_\mu(m)$ is reconstructed by using the deinterleaver, which removes the influences, that are caused by the real values of the subband transfer functions at sampling positions $n = mM + M/2$.

[1] According to Fig. 1, μ corresponds to an even numbered subband and $\kappa = 0$ represents the upper path in the interleaver.

[2] Referring to Fig. 1, ν relates to an even numbered subband and $\lambda = 0$ represents the upper path in the deinterleaver.

3 EQUALIZATION

In data transmission applications, conditions for almost perfect reconstruction, such as $c(n) = \delta(n)$ and $\eta(n) = 0$, are violated. Since we assume that the distortion in a subband is only caused by the signals within the subband and in adjacent subbands, due to the bandwidth restriction of the prototype filter, we consider three subband FIR filters to be employed for equalization of each subband signal. One subband filter is used for canceling intersymbol interferences, the others for reducing crosstalk from the adjacent subbands.

As shown in the previous chapter, the deinterleaver plays the key role in signal reconstruction at the MDFT transmultiplexer. Hence, there is a need to discuss the various possibilities for handling the deinterleaver when equalizing the transmission channel. Moreover, our system description of the MDFT transmultiplexer has shown that there is no signaling of the real and imaginary part of a complex symbol, fed into the transmitter, over the channel at the same time. Obviously, an MDFT filter bank consisting of M complex subbands can be described as a filter bank of $2 \times M$ real subbands. Therefore, we run the subband equalizer structures at sampling rate $k = 2m$. For equalization purpose, the receiver, as shown in Fig. 1, is modified by replacing the deinterleaver part by three various structures which we name as $\mathcal{A}$, $\mathcal{B}$, and $\mathcal{C}$.

In structure $\mathcal{A}$, the three subband filters are placed behind a modified deinterleaver, as shown in Fig. 2. This

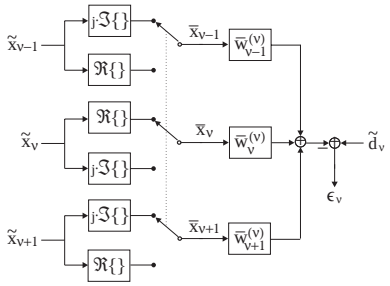

Figure 2: Equalizer structure $\mathcal{A}$. The switch turns at sampling rate $k = 2m$.

approach is already known in literature [4, 5, 6]. As reference signal, $\tilde{d}_\mu(k)$ is used, which we get as a training sequence or hard decided equalizer output (decision directed mode). The input signals of the ν'th subband equalizer $w^{(\nu)}$ are given by the real or imaginary part of the signals $\tilde{x}_{\nu-1}(k)$, $\tilde{x}_\nu(k)$, and $\tilde{x}_{\nu+1}(k)$. More precisely, by representing the signals as vectors, we get

$$\bar{\boldsymbol{y}}^t(k) \stackrel{\triangle}{=} \left(\bar{x}_{\nu-1}(k), \bar{x}_\nu(k), \bar{x}_{\nu+1}(k)\right), \quad (8)$$

$$\bar{\boldsymbol{x}}^t(k) \stackrel{\triangle}{=} \left(\bar{\boldsymbol{y}}^t(k), \bar{\boldsymbol{y}}^t(k-1), \ldots, \bar{\boldsymbol{y}}^t\left(k-(L-1)\right)\right), \quad (9)$$

$$\bar{\boldsymbol{w}}^t(k) \stackrel{\triangle}{=} \Big(\bar{w}^{(\nu)}_{\nu-1,0}(k), \bar{w}^{(\nu)}_{\nu,0}(k), \bar{w}^{(\nu)}_{\nu+1,0}(k), \ldots, \bar{w}^{(\nu)}_{\nu-1,L-1}(k), \bar{w}^{(\nu)}_{\nu,L-1}(k), \bar{w}^{(\nu)}_{\nu+1,L-1}(k)\Big), \quad (10)$$

where L denotes the length of each equalizer subband filter $w_\mu^{(\nu)}$. Using Eqs. (9) and (10), the equalization error can be written as

$$\epsilon_\nu(k) = \tilde{d}_\nu(k) - \bar{\boldsymbol{w}}^t(k)\bar{\boldsymbol{x}}(k) = \tilde{d}_\nu(k) - \bar{\boldsymbol{x}}^t(k)\bar{\boldsymbol{w}}(k). \quad (11)$$

Eq. (11) is very similar to the standard problem formulation for equalization in the well known single-band case. Therefore, the Wiener solution and the LMS adaptive algorithm do not need to be derived here.

We propose a new strategy, where we place the filters in front of the deinterleaver. There are two possibilities to provide such a structure with a reference signal. As one possibility, which we name as equalizer structure $\mathcal{B}$, we consider $\tilde{d}_\mu(k)$ as reference signal, so that we have to modify the output signal of the equalizer filters as shown in Fig. 3.

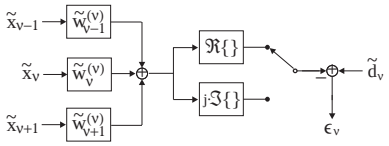

Figure 3: Equalizer structure $\mathcal{B}$. Again, the switch turns at double the symbol rate $k = 2m$.

For deriving the Wiener solution and LMS adaptive algorithm for structure $\mathcal{B}$, we define vectors similarly as for structure $\mathcal{A}$. For that, in Eqs. (8), (9) and (10) we just have to replace the bar by a tilde to be compliant with our notation. By defining $k = 2m - \lambda$, where $\lambda \in \{0, 1\}$[3], the equalization error for structure $\mathcal{B}$ is given by

$$\epsilon_\nu(k) = \tilde{d}_\nu(k) - \frac{1}{2}\Big(\tilde{\boldsymbol{w}}^t(k)\tilde{\boldsymbol{x}}(k) + (-1)^{\nu+\lambda}\tilde{\boldsymbol{w}}^\dagger(k)\tilde{\boldsymbol{x}}^*(k)\Big) \quad (12)$$

Defining abbreviations as follows

$$\sigma_d^2 \triangleq E\Big\{|\tilde{d}_\nu(k)|^2\Big\}, \quad (13)$$

$$\tilde{\boldsymbol{p}} \triangleq E\Big\{\tilde{\boldsymbol{x}}^*(k)\tilde{d}_\nu(k)\Big\} = E\Big\{(-1)^{\nu+\lambda}\tilde{\boldsymbol{x}}^*(k)\tilde{d}_\nu^*(k)\Big\}, \quad (14)$$

$$\tilde{\boldsymbol{R}} \triangleq E\big\{\tilde{\boldsymbol{x}}^*(k)\tilde{\boldsymbol{x}}^t(k)\big\}, \quad (15)$$

$$\tilde{\boldsymbol{S}} \triangleq E\big\{(-1)^{\nu+\lambda}\tilde{\boldsymbol{x}}(k)\tilde{\boldsymbol{x}}^t(k)\big\}, \quad (16)$$

the mean squared equalization error can be written as

$$\begin{aligned}\sigma_{MSE}^2 &= E\{\epsilon_\nu^*(k)\epsilon_\nu(k)\} \\ &= \sigma_d^2 - \frac{1}{2}\Big(\tilde{\boldsymbol{w}}^\dagger\tilde{\boldsymbol{p}} + \tilde{\boldsymbol{w}}^t\tilde{\boldsymbol{p}}^* + \tilde{\boldsymbol{p}}^\dagger\tilde{\boldsymbol{w}} + \tilde{\boldsymbol{p}}^t\tilde{\boldsymbol{w}}^*\Big) + \cdots \\ &\quad + \frac{1}{4}\Big(\tilde{\boldsymbol{w}}^\dagger\tilde{\boldsymbol{R}}\tilde{\boldsymbol{w}} + \tilde{\boldsymbol{w}}^\dagger\tilde{\boldsymbol{S}}^*\tilde{\boldsymbol{w}}^* + \tilde{\boldsymbol{w}}^t\tilde{\boldsymbol{S}}\tilde{\boldsymbol{w}} + \tilde{\boldsymbol{w}}^t\tilde{\boldsymbol{R}}^*\tilde{\boldsymbol{w}}^*\Big). \quad (17)\end{aligned}$$

Taking into account that transposing a scalar does not change its value we get

$$\begin{aligned}\sigma_{MSE}^2 &= \sigma_d^2 - \Big(\tilde{\boldsymbol{w}}^\dagger\tilde{\boldsymbol{p}} + \tilde{\boldsymbol{w}}^t\tilde{\boldsymbol{p}}^*\Big) + \cdots \\ &\quad + \frac{1}{4}\Big(\tilde{\boldsymbol{w}}^\dagger\tilde{\boldsymbol{R}}\tilde{\boldsymbol{w}} + \tilde{\boldsymbol{w}}^\dagger\tilde{\boldsymbol{S}}^*\tilde{\boldsymbol{w}}^* + \tilde{\boldsymbol{w}}^t\tilde{\boldsymbol{S}}\tilde{\boldsymbol{w}} + \tilde{\boldsymbol{w}}^t\tilde{\boldsymbol{R}}^*\tilde{\boldsymbol{w}}^*\Big) \\ &= \sigma_d^2 - 2\Re\Big\{\tilde{\boldsymbol{w}}^\dagger\tilde{\boldsymbol{p}}\Big\} + \frac{1}{2}\Re\Big\{\tilde{\boldsymbol{w}}^\dagger\tilde{\boldsymbol{R}}\tilde{\boldsymbol{w}} + \tilde{\boldsymbol{w}}^\dagger\tilde{\boldsymbol{S}}^*\tilde{\boldsymbol{w}}^*\Big\}. \quad (18)\end{aligned}$$

By defining the complex gradient as

$$\frac{\partial\sigma_{MSE}^2}{\partial\tilde{\boldsymbol{w}}} \triangleq \frac{\partial\sigma_{MSE}^2}{\partial\tilde{\boldsymbol{w}}_r} + j\frac{\partial\sigma_{MSE}^2}{\partial\tilde{\boldsymbol{w}}_i}, \quad (19)$$

Eq. (18) reads

$$\frac{\partial\sigma_{MSE}^2}{\partial\tilde{\boldsymbol{w}}} = -2\tilde{\boldsymbol{p}} + \tilde{\boldsymbol{R}}\tilde{\boldsymbol{w}} + \tilde{\boldsymbol{S}}^*\tilde{\boldsymbol{w}}^*. \quad (20)$$

In order to obtain the Wiener solution by setting the gradient to zero, we have to separate the complex matrices into their real and imaginary part and we can write a system of two matrix equations which is solved by

$$\begin{bmatrix}\tilde{\boldsymbol{w}}_r \\ \tilde{\boldsymbol{w}}_i\end{bmatrix} = \begin{bmatrix}(\tilde{\boldsymbol{R}}_r + \tilde{\boldsymbol{S}}_r) & -(\tilde{\boldsymbol{R}}_i + \tilde{\boldsymbol{S}}_i) \\ (\tilde{\boldsymbol{R}}_i - \tilde{\boldsymbol{S}}_i) & (\tilde{\boldsymbol{R}}_r - \tilde{\boldsymbol{S}}_r)\end{bmatrix}^{-1}\begin{bmatrix}2\tilde{\boldsymbol{p}}_r \\ 2\tilde{\boldsymbol{p}}_i\end{bmatrix}. \quad (21)$$

A gradient algorithm for minimizing σ_{MSE}^2 can be formulated as

$$\tilde{\boldsymbol{w}}(k+1) = \tilde{\boldsymbol{w}}(k) - \frac{\beta}{2}\frac{\partial\sigma_{MSE}^2}{\partial\tilde{\boldsymbol{w}}(k)}. \quad (22)$$

Using Eqs. (12) and (20), the gradient can be written

$$\begin{aligned}\frac{\partial\sigma_{MSE}^2}{\partial\tilde{\boldsymbol{w}}(k)} &= E\big\{-2\tilde{\boldsymbol{x}}^*(k)\tilde{d}_\nu(k) + \tilde{\boldsymbol{x}}^*(k)\tilde{\boldsymbol{x}}^t(k)\tilde{\boldsymbol{w}}(k) + \cdots \\ &\quad + (-1)^{\nu+\lambda}\tilde{\boldsymbol{x}}^*(k)\tilde{\boldsymbol{x}}^\dagger(k)\tilde{\boldsymbol{w}}^*(k)\big\} \\ &= -2E\{\tilde{\boldsymbol{x}}^*(k)\epsilon_\nu(k)\}. \quad (23)\end{aligned}$$

For the LMS adaptive algorithm the expected value is approximated by $E\{\tilde{\boldsymbol{x}}^*(k)\epsilon_\nu(k)\} \doteq \epsilon_\nu(k)\tilde{\boldsymbol{x}}^*(k)$ and $\tilde{\boldsymbol{w}}(k+1) = \tilde{\boldsymbol{w}}(k) + \beta\epsilon_\nu(k)\tilde{\boldsymbol{x}}^*(k)$ follows.

Finally, another possibility, which we call equalizer structure $\mathcal{C}$, is given by the usage of the signal $\tilde{x}_\nu(k)$ as reference signal, that the transmultiplexer would produce having satisfied the conditions of almost perfect reconstruction, as shown in Fig. 4. In this case, no deinterleaver is used. The reference signal has to be generated running the entire MDFT transmultiplexer filter bank using a training sequence or hard decided equalizer output.

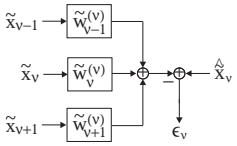

Figure 4: Equalizer structure $\mathcal{C}$. The signal $\hat{\tilde{x}}_\nu(k)$ represents the output signal of the MDFT transmultiplexer with conditions for almost perfect reconstruction.

The problem formulation for equalizer structure $\mathcal{C}$ is very similar to the single-band case. Therefore, we skip again the derivation of the Wiener solution and the LMS adaptive algorithm.

[3] According to our handling of the notation in the previous chapter, ν relates again to an even numbered subband and $\lambda = 0$ to the upper path in the modified deinterleaver, shown in Fig. 3.

4 EXPERIMENTAL RESULTS

In order to obtain the following results, various simulations are conducted, employing an 8-band MDFT transmultiplexer filter bank. The FIR filter prototype used in the filter bank design shows a stop band attenuation of 40 dB and a roll-off factor of 0.5. In all simulation results shown, for structures $\mathcal{A}, \mathcal{B}$ and $\mathcal{C}$, each equalizer's subband filter has a equalization window of $k = 5$. The results are averaged over all 8 subbands.

In Fig. 5 we present the minimum mean squared error (MMSE) when simulating the channel by a complex rotation operator $c(n) = \exp(j\varphi)$ and using additive white Gaussian noise (AWGN) with a signal-to-noise ratio (S/N) of 20 dB. Not surprisingly, the MMSE

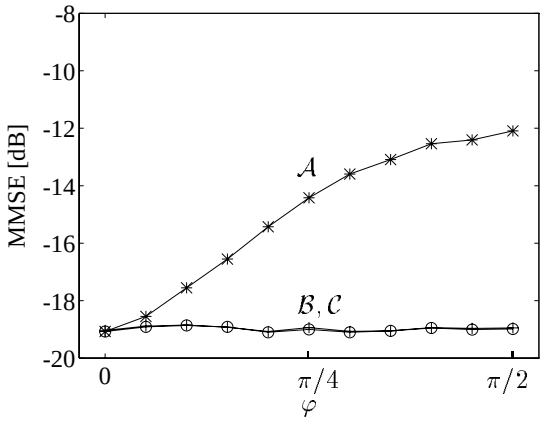

Figure 5: MMSE vs. rotation angle φ.

of structure $\mathcal{B}$ and $\mathcal{C}$ is of equal value, since these structures use the same input signal. The MMSE of equalizer structure $\mathcal{A}$ is significantly degraded, which lays bare that, if applying the deinterleaver prior to the equalization, the direction information to rotate back $c(n) = \exp(j\varphi)$ is lost. This effect is relevant in terms of synchronization issues. Assume that $c(n) = \delta(n-\Delta)$, the subband transfer function becomes $f_{\mu,\nu}(n) = \left(Mh(n)e^{j\Omega_\mu n} * h(n-\Delta)e^{j\Omega_\nu n}\right) e^{-j\Omega_\nu \Delta}$.

In Fig. 6, we demonstrate the effect of a delay, ranging from $\Delta = 0$ to $\Delta = Mn$. The received signal is corrupted again by AWGN with S/N of 20 dB.

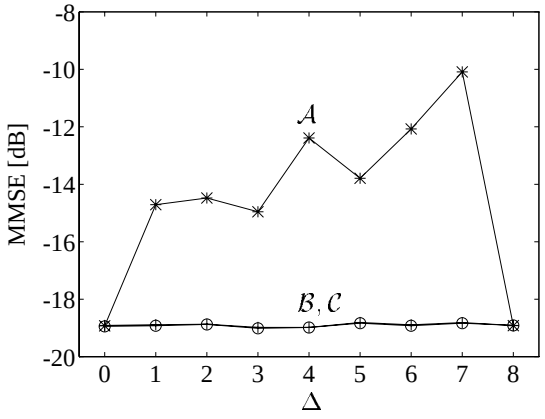

Figure 6: MMSE vs. delay.

Finally, in Fig. 7 we show the convergence behavior of the LMS adaptive algorithm when simulating the channel by an FIR filter having an impulse response $c(n) = 1 + (0.1 - j0.9)z^{-1}$ and by AWGN with S/N of 20 dB. The LMS adaptive step size is set to be the inverse of the energy of the equalizer's input vector. As expected, equalizer structure $\mathcal{C}$ provides faster convergency then structure $\mathcal{B}$, since the equalization error of $\mathcal{B}$ is modified by the deinterleaver.

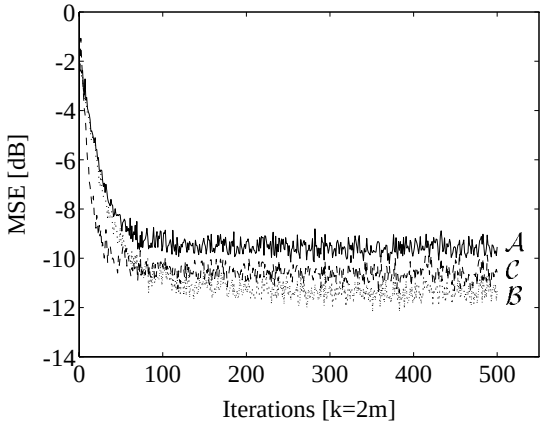

Figure 7: Convergence behavior of the LMS algorithm.

5 CONCLUSIONS

In this paper we have introduced two new FIR subband equalizer structures for channel equalization in OMC data transmission systems. The new structures have been shown to be superior to a previously known structure in terms of MMSE when computing the Wiener solution and convergence behavior of the LMS algorithm. In comparison between the two new structures, they provide equal MMSE results, since they are using the same input signal. However, the convergence behavior of the LMS algorithms in these structures is different, because of the modified adaptation rules employed.

References

[1] N.J. Fliege, "Orthogonal Multiple Carrier Data Transmission", *ETT*, vol. 3, No. 3, pp. 255–264, May 1992.

[2] G. Rösel and N. J. Fliege, "Transmultiplexer Filter Banks with Extremely Low Crosstalk and Intersymbol Interference", in *Proc. ISCAS*, Seattle, USA, 1995.

[3] N. J. Fliege, "Closed Form Design of Prototype Filters for Linear Phase DFT Polyphase Filter Banks", in *Proc. ISCAS*, Chicago, USA, May 1993, pp. 651–654.

[4] B. Hirosaki, "An Analysis of Automatic Equalizers for Orthogonally Multiplexed QAM Systems", *IEEE Trans. on Communications*, vol. COM-28, pp. 73–83, Jan. 1980.

[5] A. Mertins, *Signalverarbeitung mit Wavelets, Filterbänken und stochastischen Mehoden*, Postdoctoral thesis, Hamburg University of Technology, 1995.

[6] N.J. Fliege and G. Rösel, "Equalizers and Crosstalk Compensation Filters for DFT Polyphase Transmultiplexer Filter Banks", in *Proc. ISCAS*, London, UK, May 1994, vol. 3, pp. 173–176.